Spring 2018

Development of hollow coaxial cable Fabry Perot Resonator for high temperature sensing applications

Mohammed Farhan Ahmed

DEVELOPMENT OF HOLLOW COAXIAL CABLE FABRY PEROT RESONATOR FOR HIGH TEMPERATURE SENSING APPLICATIONS

by

MOHAMMED FARHAN AHMED

A THESIS

Presented to the Faculty of the Graduate School of the

MISSOURI UNIVERSITY OF SCIENCE AND TECHNOLOGY

In Partial Fulfillment of the Requirements for the Degree

MASTER OF SCIENCE IN ELECTRICAL ENGINEERING

2018

Approved by

Dr. Jie Huang, Advisor
Dr. Greg Hilmas
Dr. Jun Fan

PUBLICATION THESIS OPTION

This thesis has been prepared in the form of two papers:

Paper I, pages 5 to 21 has been published in IEEE Sensors Journal, vol. 17, no. 10, pp. 3052-3057, May 2017.

Paper II, pages 22 to 36 are intended for submission to IOPSCIENCE Measurement Science and Technology.

ABSTRACT

The thesis is comprised of two papers, the first paper presents the novel High-Quality Factor Coaxial Cable Fabry-Perot Resonator for sensing applications. The sensor is fabricated by creating two highly reflective mirrors in a coaxial cable. The temperature response of the sensor was tested, by monitoring the frequency shift of the reflection spectra as the temperature increased linearly from 35 °C to 80 °C in steps of 5 °C. The sensor exhibited high temperature sensitivity and good measurement resolution. A high Q factor of 133 was recorded.

The second paper in the thesis presents a low cost, robust, homemade hollow coaxial cable Fabry-Perot resonator for high temperature sensing applications. In a hollow coaxial cable, the traditional dielectric polyethylene insulator is replaced by air. This sensor is also based upon the Fabry-Perot resonator, which is fabricated by making two highly reflective mirrors in the hollow coaxial cable. The temperature response of the sensor is tested, by monitoring the frequency shift of the reflection spectra as the temperature is increased from 100 °C to 600 °C and decreased back to 100 °C in steps of 50 °C. The proposed sensor exhibited good sensitivity, stability and repeatability. For demonstration, in this paper the hollow coaxial cable was fabricated using stainless steel, but it can also be fabricated with high temperature conductive materials like tungsten, nickel, cobalt alloys, conductive ceramics, which can operate in ultra-high temperatures (e.g., up to 1600 °C).

ACKNOWLEDGMENTS

First and foremost, I am eternally gratefull to All Mighty Allah for helping me in achieving this goal.

Then, I would like to acknowledge my advisor Dr. Jie Huang. I sincerely appreciate his continuous support and devoted guidance throughout my Master's study. His meticulous commitment to research and immense hard work are the two key motivating factors that kept me going throughout my Master's study. Without his constructive suggestions, insightful comments and unconditional support this thesis would not have been possible.

I would also like to thank the members of my advisory committee, Dr. Jun Fan and Dr. Greg Hilmas, for generously offering their time and invaluable advice for my research.

I would like to thank University of Missouri Research Board for providing funds for my research.

Last but not the least, I would like to thank my siblings, parents, grandparents and friends for believing in me and supporting me throughtout these years.

TABLE OF CONTENTS

Page

PUBLICATION THESIS OPTION iii

ABSTRACT iv

ACKNOWLEDGMENTS v

SECTION

1. INTRODUCTION 1

PAPER

I. HIGH QUALITY FACTOR COAXIAL CABLE FABRY-PEROT RESONATOR FOR SENSING APPLICATION 5

ABSTRACT 5

1. INTRODUCTION 5

2. THEORY 8

3. EXPERIMENTAL SECTION 13

3.1 Fabrication of Sensor 13

3.2. Temperature Measurement 14

4. CONCLUSION 18

REFERENCES 18

II. DEVELOPMENT OF HOLLOW COAXIAL CABLE RESONATOR FOR HIGH TEMPERATURE SENSING APPICATIONS 22

ABSTRACT 22

1. INTRODUCTION 23

2. THEORY 25

3. EXPERIMENTAL SECTION 28

3.1 Fabrication of Sensor 28

3.2 Temperature Measurement 29

4. CONCLUSION 33

REFERENCES 34

SECTION

2. CONCLUSION 37

VITA 39

LIST OF ILLUSTRATIONS

Figure Page

PAPER I

1. Amplitude of Reflection and Transmission Coefficient for different shapes of reflectors. 10
2. Amplitude of Reflection coefficient as a function of frequency for a single cylindrical reflector. 11
3. Amplitude of Calculated Reflection and Transmission Spectrum. 12
4. Experimental Setup of CCFPR. 14
5. Experimental Results of Amplitude of Reflection and Transmission Spectrum. .. 15
6. Change in Reflection and Transmission spectra and their Resonant Frequencies as the temperature increases. 17
7. Measurement Resolution test at Resonant Frequency. 17

PAPER II

1. Illustration of HCC-FPR. 27
2. Experimental Setup of HCC-FPR. 28
3. Experimental Results of Reflection Spectrum. 29
4. Change in Reflection and Transmission spectra as the temperature increases. 30
5. Resonant Frequency shift of the Reflection spectra as the temperature increases and then decreases. 31
6. Measurement Resolution test at Resonant Frequency. 32
7. Resonant Frequency shift monitored at every temperature point. 33

SECTION

1. INTRODUCTION

Complex civil infrastructures, such as buildings, bridges, dams, tunnels, pipelines and offshore platforms are often subjected to severe environmental conditions and anomalous loads, e.g. strong winds, heavy rains/snowfall, high humidity and huge temperature variations that cannot be easily anticipated during the design process. This can result in long-term structural deterioration that often is not detected by conventional visual inspection. Moreover, catastrophic disasters, such as hurricanes, earthquakes, storms, tornadoes and floods can severely affect the health of the structure in a small duration which can lead to life-threatening conditions. The factors that affect the integrity of these large and complex civil infrastructures cannot be precisely predicted. For this reason, in recent years Structural Health Monitoring (SHM) technologies have emerged to real time monitor the health status of these structures. Embedded sensors have the most desired capability for SHM. These sensors are used for monitoring several structural and environmental parameters such as temperature, strain, force, vibration, corrosion, cracks, and chemical properties under ambient and extreme conditions for assessing the health of the structures.

In the past few decades, fiber optic sensors have attracted a lot of research interest in SHM applications due to their unique advantages over traditional sensors such as compactness, high resolution, remote monitoring capability, low attenuation and most significantly their immunity to electromagnetic interference. Several sensing concepts can be used to fabricate these sensors such as waveguide mode sensing, surface Plasmon resonance sensing, fiber Bragg grating (FBG) sensing, long period grating sensing and Fabry-Perot interferometric (FPI) sensing. FBG sensing is the most commonly used concept in fabrication of optic sensors for SHM due to its versatile advantages like miniature size, great durability, long term stability and easy multiplexing. FBG consists of several reflection points that reflect a particular wavelength of incident light and transmit all others. When subjected to strain or temperature, the grating period changes and a different wavelength is reflected which enables us to determine the Bragg wavelength variation.

With several unique advantages, fiber optic sensors face limitations too. They have small dynamic range (about 4000 $\mu\varepsilon$ or 0.4%) due to the limited deformability of silica glass. Even with rigorous packing, fiber optic sensors can easily break down when subjected to large strains (e.g. 1%) or a shear force, causing serious challenges for sensor installation and operation. Also, they cannot withstand temperatures higher than 800 °C, which makes them difficult to be used in high temperature harsh environments (e.g., up to 1500 °C).

Recently, people started migrating ideas from optical fibers to coaxial cables as they share the same electromagnetic theory. In comparison with optical fibers, coaxial cables can survive large strains (e.g. 4%) due to its large dimensions (~ 5 mm), also they are insensitive to lateral force or bending and most importantly they operate in TEM mode. The FBG concept has been successfully implemented on coaxial cables. Coaxial cable Bragg grating (CCBG) is fabricated by drilling open holes at periodic distance along the coaxial cable. The periodic impedance discontinuities result in resonant peaks in the reflection and transmission spectra at discrete frequencies. The spectrum shifts whenever the CCBG is subjected to any physical change or have change in their material properties, thereby acting as a sensor. The large dynamic range (50,000 $\mu\varepsilon$ or 5%), robustness, compactness and low cost provides a very promising solution for SHM. However, due to long gauge length of the CCBG, the spatial resolution (~ 1 m) is limited.

A promising solution for the high spatial problem of CCBG is inspired by the coaxial cable Fabry-Perot Interferometer (CCFPI). CCFPI consists of two reflective mirrors separated by a few centimeters along the coaxial cable. EM waves reflected at the two reflectors have different time delays resulting in an interference signal. When subjected to strain or temperature, the physical length of the cavity, or the material properties, changes resulting in a shift of the interference pattern. The shift can be used to determine the change in temperature or strain. However, the detection limit of the CCFPI is low due to the low Q factor (~ 5) of the interferometer.

To overcome the lower detection limit of the CCFPI, we have proposed a high-quality factor coaxial cable Fabry-Perot resonator (CCFPR), which is presented in the first part of the thesis. CCFPR consists of two highly reflective mirrors (> 80%) with a separation of few centimeters. EM waves travelling inside the cable gets reflected at the mirrors, resulting in a resonating pattern. When subjected to physical change or change in material properties, the transmission and reflection spectra shifts, thereby acting as a sensor. CCFPR has several advantages which made it a good fit to be used for SHM. However, CCFPR was limited by the melting point of its dielectric (150 °C), which made it difficult to be used in high temperature environments.

To address this challenge, we proposed a hollow coaxial cable Fabry-Perot resonator for high temperature sensing applications, which is presented in the second part of the thesis. In the HCC design, air is used to replace the traditional dielectric polyethylene. This resulted in eliminating the lower melting point of a traditional dielectric in the coaxial cable. Depending upon the material HCC is made up of, it can operate to temperatures as high as 1600 °C. HCC-FPR has similar working concept as CCFPR, which is based on the FPR. When subjected to physical change or change in material properties, the resonating pattern of HCC-FPR shifts, resulting in a sensor. The robust HCC-FPR temperature sensor can be easily commercialized and has great potential for sensing applications in high temperature harsh environments, thereby a good fit for SHM.

PAPER

I. HIGH QUALITY FACTOR COAXIAL CABLE FABRY-PEROT RESONATOR FOR SENSING APPLICATION

Mohammed Farhan Ahmed[1], Ting Xue[2], Bin Wu[3], and Jie Huang[1*]

[1]Department of Electrical and Computer Engineering, Missouri University of Science and Technology, Rolla, MO 65401, USA
[2]School of Electrical and Information Technology, Tianjin University, Tianjin 300072, China
[3]State Key Laboratory of Precision Measuring Technology and Instruments, Tianjin University, Tianjin 300072, China

Email: {mn64c, jieh} @mst.edu

ABSTRACT

This paper describes a novel coaxial cable Fabry-Perot resonator for sensing applications. The sensor was fabricated by creating two highly reflective mirrors in a coaxial cable. The device physics was discussed. The temperature response of the sensor was tested. The temperature measurement was achieved by monitoring the frequency shift of the reflection and transmission spectra as the temperature was increased linearly in steps of 5 °C from 35 °C to 80 °C. This sensor exhibited high temperature sensitivity and measurement resolution. Highest Q factor of 133 was recorded. It has been derived that the Q factor decreases as the frequency increases.

1. INTRODUCTION

Optical fiber sensing has been attracting many research interests for their broadband applications in the fields of chemistry, biology, biochemistry, petroleum industry, environment and medical care [1]. Optical fiber sensors have many advantages over traditional electrical sensors such as compactness, high resolution, remote monitoring capability and most significantly their immunity to electromagnetic interference [2]. Waveguide mode sensing [3-5], surface Plasmon resonance sensing

[6,7], fiber Bragg grating (FBG) sensing [8,9], long period grating sensing [10] and Fabry-Perot Interferometric (FPI) sensing [11,12] are some optical sensing concepts. The most commonly used concept is FBG due to its versatile advantages like miniature size, great durability, long term stability and easy multiplexing [13]. FBG consists of many reflection points that reflect a particular wavelength of incident light and transmit all others. When subjected to strain or temperature the grating period changes and so a different wavelength is reflected which enables us to determine the Bragg wavelength variation [14]. Recently, there has been an increase of interest in using FBG's in Structural Health Monitoring (SHM) [15].

Although with such high merits, optical fiber sensors have some limitations. They have small dynamic range due (about 4000 $\mu\varepsilon$ or 0.4%) to the limited deformability of silica glass. Even with rigorous packing, fiber sensors can easily break down when subjected to large strains (e.g. 1%) or a shear force, causing serious challenges for sensor installation and operation [16]. Consequently, the applications of optical fiber sensors are limited in heavy duty or large strain measurements which makes it difficult to be used in SHM.

In recent years, people have been migrating ideas of the optical fiber to coaxial cable as they share the same electromagnetic theory. In comparison with optical fibers, the main merit of using coaxial cable is its ability to survive large strains (more than 2%) due to its large dimension (~ 5 mm). Likewise, coaxial cables are also insensitive to lateral force or bending. The FBG concept has been successfully implemented on coaxial cables. A coaxial cable Bragg grating (CCBG) was fabricated by drilling open holes at periodic distance along the coaxial cable. The periodic impedance discontinuities produce resonant peaks in both transmission and reflection spectra at discrete frequencies. This spectrum shifts whenever the CCBG is subjected to any physical change or there is a change in their material properties. To demonstrate the ability to use a CCBG as a sensor, they also conducted strain measurements [17]. The large dynamic range (50,000 με or 5%), robustness, compactness and low cost provides a very promising solution for SHM [18, 19]. However, due to the long wavelength of the radio frequency, the CCBGs usually have a long grating length (~ 1 m) in comparison with FBGs (~ 1 cm), thus, the spatial resolution of CCBG is limited.

A promising solution for the spatial resolution problem of coaxial cable sensors is inspired by the optical Fabry-Perot resonator (FPR). FPRs typically have comparable sensitivity when compared to FBGs but for a much shorter length. FPR consists of two reflectors with a separation of hundreds of micrometers. Light waves reflected at the two reflectors have a different time delay, resulting in an interference signal. When subjected to strain or temperature the physical length, or material properties, change which lead to shifting in the interference pattern [20-23]. This shift can then be used to determine the change in temperature or strain. Finesse is a factor that is used to quantify the performance of a resonator [24, 25]. The finesse of a Fabry-Perot resonator is given by the ratio of the free spectral range to the full width at half maxima (FWHM). Finesse of Fabry-Perot varies with the reflectivity of the mirrors [26]. The smaller reflectivity of the mirror decreases the finesse whereas higher reflectivity increases the finesse. The higher the finesse, the higher the number of interfering beams which results in a more complex interference pattern and therefore high-resolution measurements [27]. The detection limit of a sensor depends on the Q factor of the resonator. Q factor is defined as the ratio of the resonance frequency to the FWHM. Higher finesse causes higher optical Q-factors, thereby increasing the detection limit of the sensor. In this paper, we proposed a high Quality factor (Q-factor) coaxial cable Fabry-Perot resonator (CCFPR) by imitating the concept of the optical Fabry-Perot resonator. Two highly reflective reflectors (< 80%) were introduced in a coaxial cable functioning as two mirrors. When the CCFPR is subjected to any physical change or it faces any change in its material properties, the reflection and transmission spectra shift from its initial position, thus making coaxial cable act as a sensor.

2. THEORY

CCFPR consists of two reflectors with very high reflectivity separated by a distance of centimeters. The EM wave traveling inside the cable gets mostly reflected at the first reflector while a small portion of the remaining energy with a phase shift gets transmitted and reaches the second reflector. At the second reflector, again a very small portion (~ 1%) of the waves gets transmitted and this repeats. The reflections are generated by impedance discontinuities because of interruption in material properties such as permittivity or permeability or in physical parameters like inductance, capacitance or resistance. Even though there are two reflectors with very high reflectivity here, still the transmission at particular resonant wavelengths is 1. These wavelengths are those when the phase shift is equal to $2n\pi$. Then these partial waves travel back and forth in the cavity. The phase delay between two partial waves, which is attributed to one additional double trip is given by:

$$\delta = \frac{4\pi d \cdot \cos\theta}{\lambda} = \frac{4\pi f d\sqrt{\varepsilon_r} \cdot \cos\theta}{c} \tag{1}$$

where v is the phase velocity; f is the frequency of the EM wave travelling inside the cable; θ is the angle between the transmitted and the incident wave; ε_r is the relative permittivity of the inner dielectric material of the cable, d is the length of resonant cavity and c is the speed of light in vacuum. As coaxial cable is a transmission line, θ can be considered as zero.

The resonant transmission frequencies can be written as:

$$f_m = m\frac{v}{2d} \tag{2}$$

where m is an integer. For infinite reflections using geometric series, the reflection coefficient can be defined as:

$$\hat{R} = \frac{\sqrt{R}(e^{j\delta}-1)}{1-R^{j\delta}} \tag{3}$$

For infinite transmissions using the geometric series, the transmission coefficient can be defined as:

$$\hat{T} = \frac{(1-R)\cdot e^{-j\delta}}{1-\mathrm{Re}^{j\delta}} \tag{4}$$

where R and T are the fractions of intensity reflected and transmitted at each mirror interface i.e. the mirror's reflectance and transmittance. The amplitude of the reflected electric field and transmitted electric field using Euler's formulae can be further reduced to:

$$r = \sqrt{\frac{R[((\cos\delta-1)(1+R))^2+(\sin\delta(1-R))^2]}{(1+R^2-2R\cos\delta)^2}}$$

$$t = \sqrt{\frac{(1-R)\ [(\cos\frac{\delta}{2}(1-R\cos\delta)+R\sin\delta\sin\frac{\delta}{2}))^2+(\sin\frac{\delta}{2}(R\cos\delta-1)+R\sin\delta\cos\frac{\delta}{2}))^2]}{(1+R^2-2R\cos\delta)^2}} \tag{5}$$

The theory of FPR is well known and can be found in many books [28-30]. In this paper, we have accounted total FPR losses only to mirrors and assumed no wave propagation loss due to complex refractive index. Therefore, phase delay accounts only for the delay between two partial waves, which can easily be calculated from Eq. 1. In Eq. 5, the only unknown parameter is R. A highly reflective reflector can be generated by introducing an impedance discontinuity in a coaxial cable. This impedance discontinuity can be formed using various methods. For instance, we can create copper reflectors. Copper is used to short the inner conductor of the coaxial cable with the outer conductor of the coaxial cable thereby achieving very high reflectivity. They can be of different shapes like cylindrical, conical, cubical, spherical and rectangular. To choose the best reflector shape for our purpose, reflection coefficient of all these reflectors was simulated using HFSS. The plot of reflection and transmission coefficients as a function of frequency is shown in Fig. 1(a) and 1(b). It can be inferred from the plots that reflectivity is influenced by the different shape of reflectors. For all the reflectors, reflectivity decreases as the frequency increases. Due to differences in dimensions, the results can only provide a qualitative comparison. A cubical shaped reflector has the lowest reflectivity and the rectangular mirror has the highest. The fundamental reason for these relations deserves a detailed investigation in the future, but we are not going to cover it in this paper.

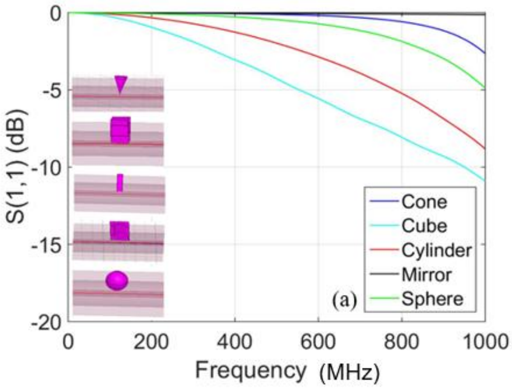

(a) Amplitude of Reflection Coefficient

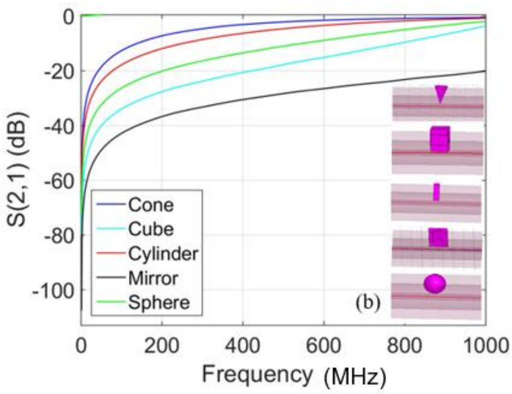

(b) Amplitude of Transmission Coefficient

Figure 1. Amplitude of Reflection and Transmission Coefficient for different shapes of reflectors.

In our research, a simple cylindrical hole was made from the outer conductor to the inner conductor of a coaxial cable and filled with copper so that a short circuit can take place and thereby creating a mirror with very high reflectivity. The coaxial cable was 15 cm long with a diameter of 0.7 cm and the cylindrical reflector was 0.8 cm in height and 0.15 cm in diameter. The reflection coefficient was numerically simulated using HFSS including the magnitude and the phase at discrete frequencies. A single cylindrical reflector with a diameter of 0.15 cm and height 0.8 cm was used to compute the reflection coefficient. Fig. 2 plots the amplitude of reflection coefficient of CCFPR as a function of frequency.

To numerically calculate the amplitude of the reflected wave and transmitted wave of a CCFPR, the relative permittivity of the dielectric material was set to 2.25 and the frequency was from 0 to 6 GHz. The distance between the two reflectors was 9.3 cm. By substituting the calculated reflection coefficient (R) of a single reflector, the reflection and transmission coefficient of a typical CCFPR were calculated based on Eq. 5 and plotted in Fig. 3. Within the observation bandwidth, five resonant dips can be seen with the fundamental frequency at 1.075GHz.

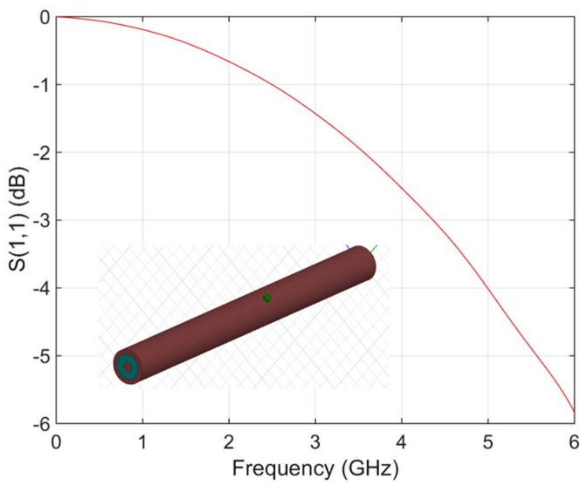

Figure 2. Amplitude of Reflection coefficient as a function of frequency for a single cylindrical reflector.

The reflectivity decreases as the frequency increases. This can be qualitatively explained by looking at Fig 2. In the simulated reflection spectra, the resonant peak has an increasing strength (till the fourth harmonic) and then decreases slightly in the fifth harmonic. For each resonant peak and dip a Q factor has been indicated in Fig 3. (a) and (b). For simulation purpose, a lossy cable was assumed while plotting the reflection and transmission spectra. The attenuation constant was calculated as a function of frequency. The mirror's reflectance was multiplied with the attenuation constant to incorporate the loss to the cable, and this value of R was substituted in Eq. 3, 4 and 5.

$$R = R.k$$

$$k = e^{-\alpha} \tag{6}$$

where k is the attenuation constant and α is the attenuation in Np/m (Nepers/meter). It can be seen that the Q factor decreases as the frequency increases (Fig 3 (a) and (b)). It is because of the higher loss cables incorporate at higher frequencies and also due to low reflectivity at higher frequencies.

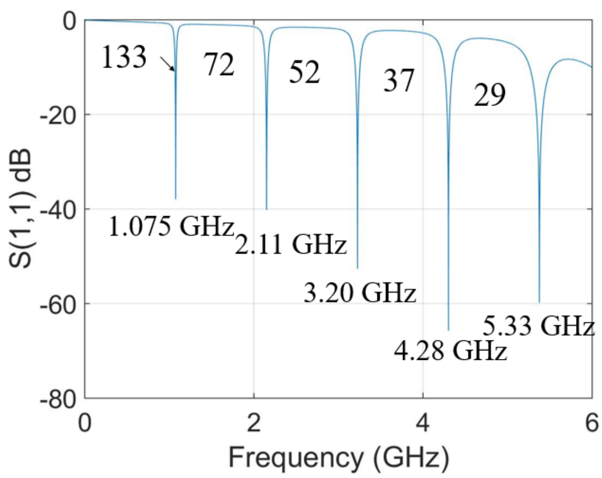

(a) Reflection Spectrum

Figure 3. Amplitude of Calculated Reflection and Transmission Spectrum.

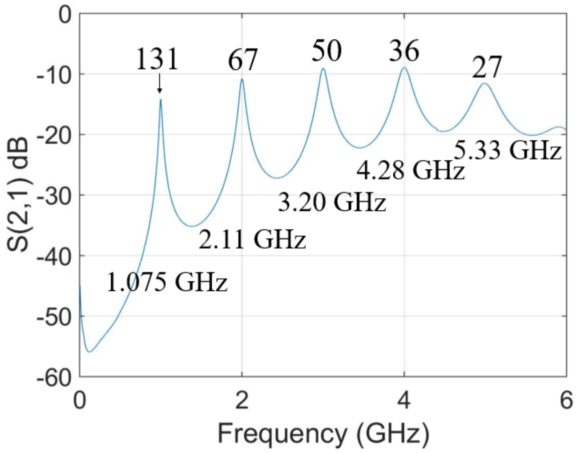

(b) Transmission Spectrum

Figure 3. Amplitude of Calculated Reflection and Transmission Spectrum. (cont.)

3. EXPERIMENTAL SECTION

3.1 Fabrication of Sensor

In order to create highly reflective mirrors, two holes were drilled into a coaxial cable (50Ω,) using a drilling machine (Black & Decker DR260B 5.2-Amp 3/8-Inch Drill/Driver). The distance between the two holes was 9.3 cm. A drilling bit of 0.25-inch diameter was used. The drilling depth was 2.29 mm and the diameter of the cable was 4.94 mm. After the drilling was completed, copper powder (Sigma-Aldrich chemistry, copper powder, <425μm, 99.5% trace metals basis) was added into the holes to create a short circuit. By understanding the boundary conditions in electromagnetics, we can say that these two holes filled with copper powder will now act as very highly reflective mirrors. These holes were then sealed by heating the jacket, such that it can be molded in closing the holes. A vector network analyzer (VNA HP8753ES) was used to monitor the reflection spectrum during the fabrication process. The VNA was configured for an observation bandwidth from 10 kHz to 6 GHz, a total of 1601 sampling points and an intermediate frequency bandwidth of 300 Hz. All the machines used in this experiment were controlled using a laptop. Figure 4 depicts the experimental setup.

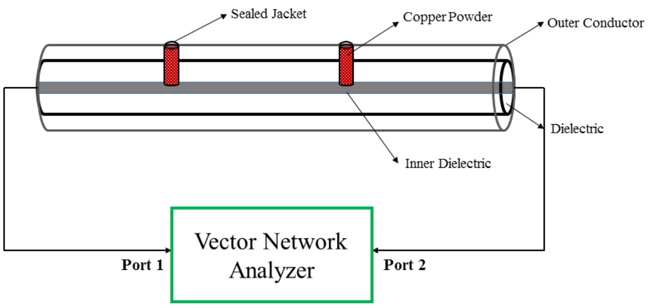

Figure 4. Experimental Setup of CCFPR.

Figure 5 (a) and (b) indicates the plots of the measured reflection and transmission spectrum of a CCFPR. Multiple resonant frequencies can be observed including the fundamental and harmonics. The Q factors and resonant frequencies are indicated in the plot for each resonant dip and peak. Several ripples can be observed in Fig 5 (a) and (b). This is due to the multiple reflections incurred from the ports of VNA. The Q factor approximately matches with the calculated data indicating this drilling method does not add any extra loss to the cable. The resonant frequencies are also the same.

3.2. Temperature Measurement

To exhibit the capability of using CCFPR as a sensing device in SHM, temperature measurement was conducted. The CCFPR used for temperature measurement also had a distance of 9.3cm. The VNA was configured to acquire the resonant frequency of approximately 2.18 GHz with an observation bandwidth from 2.13 GHz to 2.25 GHz. The resonant frequency with the highest Q factor wasn't chosen due to its low fringe visibility. The CCFPR was immersed in a beaker of distilled

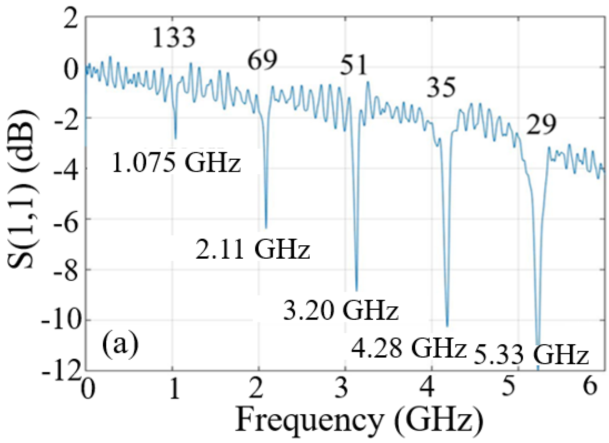

(a) Amplitude of Reflection Spectrum

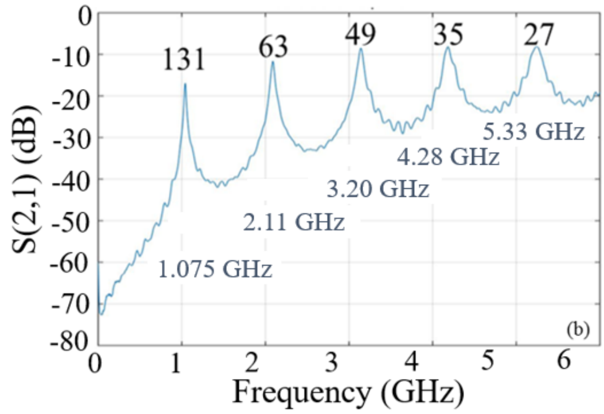

(b) Amplitude of Transmission Spectrum

Figure 5. Experimental Results of Amplitude of Reflection and Transmission Spectrum.

water and then placed on a ceramic heater. The temperature was increased from $35^{\circ}C$ to $80^{\circ}C$ with an increasing step of $5^{\circ}C$. For each temperature point, the reflection and transmission spectrum was measured.

Figure 6 (a) and (c) indicates the shift in reflection and transmission spectra as the temperature increases whereas Figure 6 (b) and (d) indicates the change in resonant frequency as a function of temperature. The resonant frequency shift with temperature is the same for both the reflection and transmission spectra. This is advantageous as either one of them can be used for monitoring, during sensing operations. The frequency shift of the spectra corresponding to a change in temperature can be explained by the following equation.

$$\frac{\Delta f}{\Delta T} = (\sigma + \alpha_{CTE}) \cdot f_n \ (Hz / ^\circ C) \tag{7}$$

where Δf is the change in frequency, ΔT is the change in temperature, σ is the temperature induced relative permittivity change, α_{CTE} is the coefficient of thermal expansion of dielectric and f_n is the nth resonant frequency. The spectra shift towards higher frequency regions indicating that the effective electrical length increases as the temperature increases. The effective electrical length is related to the physical length between the two reflectors and the relative permittivity of the inner dielectric layer. The coefficient of thermal expansion for polyethylene is -2x10^{-4} (m/(mK)). The temperature induced relative permittivity change decreases as the temperature increases, but it is still larger than the coefficient of thermal expansion. This indicates the dominance of temperature induced relative permittivity change when a CCFPR is subjected to temperature measurements. At high temperatures, the Q factor decreases due to the increase of propagation loss between the two highly reflective reflectors and also due to low reflectivity at higher frequencies. The resonant frequency increases non-linearly as the temperature increases. The higher the temperature, the larger the temperature sensitivity becomes. The average temperature sensitivity of the CCFPR was calculated to be 1.4 MHz/°C, demonstrating that this developed CCFPR can be used as a high temperature sensor with good sensitivity. The stability of CCFPR was also characterized. The resonant frequency of the sensor was constantly recorded every 30 seconds for an hour, which is shown in Figure 7. The standard deviation was calculated to be approximately ± 20 kHz or a relative measurement resolution of 4×10^{-6} around 5.93 GHz. The results show the stability of the proposed sensor for temperature measurements.

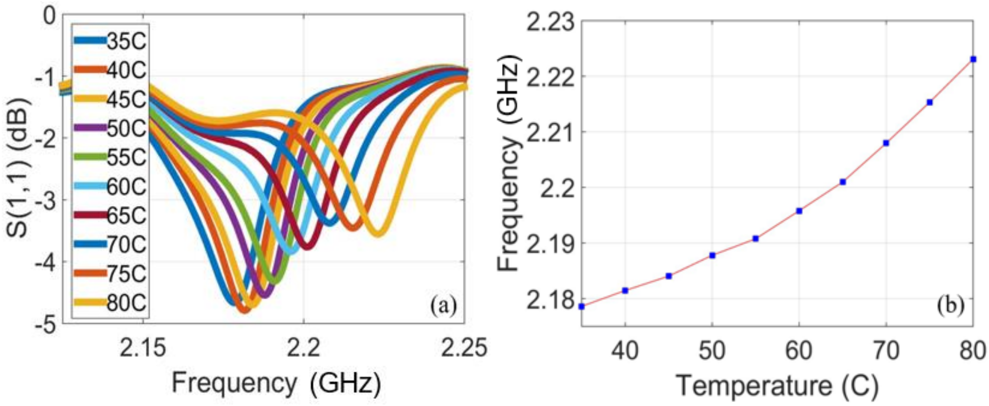

(a) Change in Reflection spectra as the ambient temperature increases. (b) Resonant frequency shift of the reflection spectra as a function of temperature.

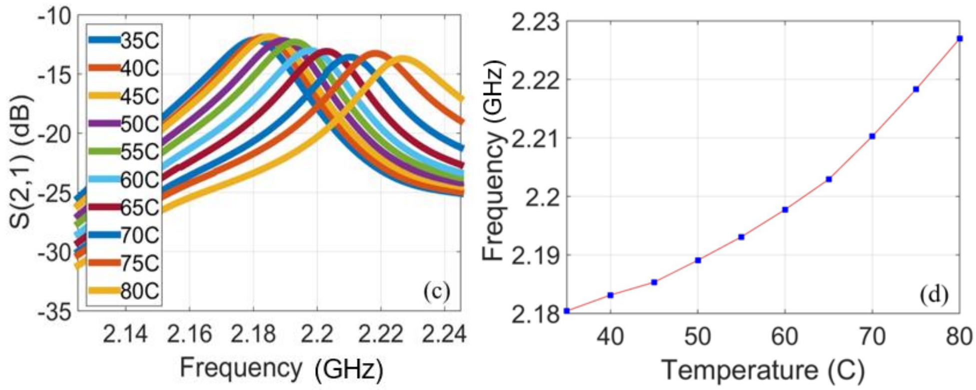

(c) Change in transmission spectra as the ambient temperature increases. (d) Resonant Frequency shift of the transmission spectra as a function of temperature.

Figure 6. Change in Reflection and Transmission spectra and their Resonant Frequencies as the temperature increases.

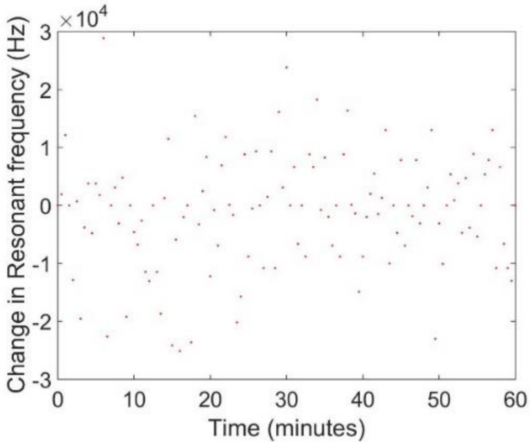

Figure 7. Measurement Resolution test at Resonant Frequency.

4. CONCLUSION

This paper presents a CCFPR, which was fabricated by drilling two holes in a coaxial cable and filling them with copper powder to create two highly reflective mirrors. These holes result in an impedance discontinuity and the short circuit due to the metallic powder results in very high reflections of the EM wave traveling inside the cable. The transmission is one at resonant frequencies though there are two highly reflective mirrors in the transmission line. The reflection coefficient of the holes was calculated using finite element method, and the device was modeled based on electromagnetic theory. All the theoretical calculations matched the experimental results well. The fabricated sensor had a Q factor of 133, and a measurement resolution of 4×10^{-6} was recorded. Temperature measurements of CCFPR were experimentally demonstrated. The average temperature sensitivity of the sensor was approximately 1.4 MHz/ºC. We have used cylindrical reflectors for fabrication of CCFPR in this experiment, different shapes and sizes of reflectors can also be used for fabrication of CCFPR. Though this paper was focused on using CCFPR for temperature sensing, it can also be used for strain and other types of sensing applications using different mechanical designs. CCFPR has many advantages like low cost, robustness, high sensitivity, high measurement resolution, high detection limit, and large strain capability. These unique features can make CCFPR of great use in SHM.

REFERENCES

[1] Sofyan A. Taya and Taher M. El-Agez, “Optical sensors based on Fabry-Perot resonator and fringes of equal thickness structure,” *Optik-Int. J. for Light and Electron Opt.*, vol. 123, no. 5, pp. 417-421, Mar 2012.

[2] M. Li, M. Wang and H. Li, “Optical MEMS pressure sensor based on Fabry-Perot interferometry,” *Opt.* Express, vol. 14, no. 4, pp. 1497-1504, 2006.

[3] D. K. Qing and I.Yamaguchi, “Analysis of the sensitivity of optical waveguide chemical sensors for TM modes by the group-index method,” *J. Opt. Soc. Am. B*, vol. 16, no. 9, pp. 1359-1369, 1999.

[4] J. Ctyroky, J. Homola and M. Skalsky, “Modelling of surface plasmon resonance waveguide sensor by complex mode expansion and propagation method,” *Opt. and Quantum. Elec.*, vol. 29, no. 2, pp. 301-311, Feb 1997.

[5] R. Horvath, H. C. Pederson and N. B. Larsen, “Demonstration of reverse symmetry waveguide sensing in aqueous solutions,” *App. Phys. Lett.*, vol. 81, no. 12, pp. 2166-2168, Sep 2002.

[6] J. Dostalek and J. Homola, “Surface plasmon resonance sensor based on array of diffraction gratings for highly parallelized observation of biomolecular interactions,” *Sensor Actuators B*, vol. 129, no. 1, pp. 303-310, Jan 2008.

[7] F. C. Chien and S. J. Chen, “A sensitivity comparison of optical biosensors based on four different surface plasmon resonance modes,” *Biosensors and Bioelectronics*, vol.20, no. 3, pp. 633-642, Oct 2004.

[8] Y. Dai, Y. Liu, J. Leng, G. Deng and A. Asundi, “A novel time-division multiplexing fiber Bragg grating sensor interrogator for structural health monitoring,” *Opt. Lasers Eng.*, vol. 47, no. 10, pp.1028-1033, Oct 2009.

[9] J. Albert, L. Y. Shao and C. Caucheteur, “Tilted fiber Bragg grating sensors,” *Lasers and Phot. Review*, vol. 7, no. 1, pp. 83-108, Feb 2012.

[10] N. Ni, C.C. Chan, W.C. Wong, L.Y. Shao, X.Y. Dong and P. Shum, “Cavity ring-down long period grating pressure sensor,” *Sensors Actuators A*, vol. 158, no. 2, pp. 207-211, Mar 2010.

[11] J. Liu, Y. Sun and X. Fan, “Highly versatile fiber-based optical Fabry-Perot gas sensor,” *Opt. Express*, vol. 17, no. 4, pp. 2731-2738, Feb 2009.

[12] H. Sun, X. Zhang, L. Yuan, L. Zhou, X. Qiao and M. Hu, “An optical fiber Fabry-Perot interferometer sensor for simultaneous measurement of relative humidity and temperature,” *IEEE Sensors J.*, vol. 15, no. 5, pp. 2891-2897, May 2015.

[13] A. Cusano, A. Antonello and J. Albert, “Fiber Bragg Grating Sensors: A Look Back,” *in Fiber Bragg Grating Sensors: recent advancements, industrial applications and market exploitation*, pp. 2-5, Apr 2011.

[14] K. O. Hill and G. Meltz, “Fiber Bragg grating technology fundamentals and overview,” *J. of Lightwave Tech.*, vol. 15, no. 8, pp. 1263-1276, Aug 1997.

[15] J. M. Lopez-Higuera, L. R. Cobo, A. Q. Incera and A. Cobo, “Fiber optic sensors in structural health monitoring,” *J. of Lightwave Tech.*, vol. 29, no. 4, pp. 587-608, Feb 2011.

[16] E. J. Friebele, “Fiber Bragg grating strain sensors: present and future applications in smart structures,” *Opt, and Phot. News*, vol. 9, no. 8, pp. 33-37, 1998.

[17] T. Wei, S. Wu, J. Huang, H. Xiao, and J. Fan, “Coaxial cable Bragg grating,” *App. Phy. Lett.*, vol. 99, no. 11, pp. 113517(1-3), 2011.

[18] J. Huang, T. Wei, X. Lan, J. Fan and H. Xiao, “Coaxial cable Bragg grating sensors for large strain measurements with high accuracy,” *Sensors and Smart Structure Technologies for Civil, Mechanical and Aerospace Systems*, Apr 2012.

[19] J. Huang, T. Wei, S. Wu, X. Lan and J. Fan, “Coaxial cable Bragg grating sensors for structural health monitoring,” *Int. J. of Pavement Res. And Tech.*, vol. 5, no. 5, pp. 338-342, Sep 2012.

[20] M. Han, Y. Zhang, F. Shen, G. R. Pickrell and A. Wang, “Signal processing algorithm for white-light optical fiber extrinsic Fabry-Perot interferometric sensors,” *Opt. Lett.*, vol. 29, no. 15, pp. 1736-1738, 2004.

[21] J. Huang, L. Hua, X. Lan, T. Wei and H Xiao, “Microwave assisted reconstruction of optical interferograms for distributed fiber optic sensing,” *Opt. Express*, vol. 21, no. 15, pp. 18152-18159, 2013.

[22] T. Wei, Y. Han, H. L. Tsai and H. Xiao, “Miniaturized fiber inline Fabry-Perot interferometer fabricated with a femtosecond laser,” *Opt. Lett.*, vol. 33, no. 6, pp. 536-538, Mar 2008.

[23] J. Huang, T. Wang, L. Hua, J. Fan, H. Xiao and M. Luo, “A coaxial cable Fabry-Perot interferometer for sensing applications,” *Sensors 2013*, vol. 13, no. 11, pp. 15252-15260, Nov 2013.

[24] Hunger, T. Steinmetz, Y. Colombe, C. Deutsch, T. W. Hansch and J. Reichel, “A fiber Fabry-Perot cavity with high finesse,” *New J. of Phy.*, vol. 12, pp. 1-24, Jun 2010.

[25] J. Poirson, F. Bretenaker, M. Vallet and A. L. Floch, “Analytical and experimental study of ringing effects in a Fabry-Perot cavity. Application to measurement of high finesse,” *J. of Opt. Soc. of Am. B*, vol. 14, no. 11, pp. 2811-2817, Nov 1997.

[26] María del Mar Sánchez-López, Jeffrey A. Davis, and Karlton Crabtree , “Coaxial Cable analogs of multilayer dielectric optical coatings,” *American J. of Physics*, vol. 71, no. 12, pp. 1314-1319, Dec 2013.

[27] G. Gaborit, G. Martin, J. L. Coutaz, L. Duvillaret, S. Kassi, D. Romanini, “High-finesse Fabry-Perot electro-optic sensors with enhanced sensitivity and high spatial resolution,” *App. Opt.*, vol. 46, no. 11, pp. 2001-2009, Apr 2007.

[28] A. Yariv, “Introduction to Optical Electronics”, Chap. 4, *Holt, Rinehart and Winston*, 1971.

[29] Yeh,Pochi, “Optical Waves in Layered Media”, Chap. 5 and 6, *Wiley* 1988.

[30] Macleod,H.A., “Thin-Film Optical Filters”, Chap. 5, *Institute of Physics Publishing*, 2001.

II. DEVELOPMENT OF HOLLOW COAXIAL CABLE RESONATOR FOR HIGH TEMPERATURE SENSING APPICATIONS

Mohammed Farhan Ahmed, Yiyang Zhuang and Jie Huang

Department of Electrical and Computer Engineering

Missouri University of Science and Technology, Rolla, MO 65409, USA

(email: {mn64c, jieh}@mst.edu)

ABSTRACT

This paper describes a low cost, robust, homemade hollow coaxial cable Fabry Perot resonator (HCC-FPR) for high-temperature sensing applications. In HCC, the traditional dielectric insulating layer is replaced by air. The sensor is fabricated by creating two highly reflective mirrors in the proposed HCC. A metal post shorting inner and outer conductor and a metal disk welded onto the end of HCC serve as two highly reflective mirrors. The device physics was discussed. The temperature response of the sensor was tested. The temperature measurement is achieved by monitoring the frequency shift of the reflection spectra as the temperature increases linearly in steps of 50 °C from 100 °C to 600 °C and decreases back to 100 °C. This sensor exhibited good sensitivity, repeatability, and stability. It should be noted that, although stainless steel was used in our initial sensor prototype, the sensor materials can be flexibly changed to other high-temperature conductive materials such as tungsten, nickel and cobalt alloy metals, or conductive ceramics, which we believe can survive ultrahigh temperatures (e.g., up to 1600 °C). The robust and easy to fabricate HCC-FPR temperature sensor can be easily commercialized and has great potential for sensing applications in high-temperature harsh environments.

1. INTRODUCTION

In the past few decades, numerous optical fiber high-temperature sensors have been developed due to their miniature design, immunity to electromagnetic interference, excellent stability, and durability. [1], [2] Waveguide mode sensing [3]-[5], surface Plasmon resonance sensing [6], [7], fiber Bragg grating (FBG) sensing [8], [9], long period grating sensing [10]- [12] and Fabry-Perot interferometric (FPI) sensing [13]- [15] are some of the optical sensing concepts . The advantages of fiber optic sensors over electronic sensors, particularly in environments where the electronic sensing materials cannot withstand the rigors of the harsh conditions, are well known [16]. Typically, advanced power generation systems operate at higher temperatures (e.g., up to 1300 °C) and pressures than traditional power plants. Traditional sensor technology for measuring temperature, pressure, flow, and strain will not survive the harsh conditions anticipated in these plants. Furthermore, these plants will require more extensive process monitoring and condition assessment to maintain optimum performance and minimize maintenance costs. Although silica glass optical fiber has several advantages, it cannot survive at temperatures above 800 °C due to the migration of dopants in a fiber core at high temperatures.

A possible solution for silica’s low melting point (i.e. 600 °C) is a sapphire fiber. They have better stability and can survive at very high temperatures (~ 1800 °C) [17] - [20]. However, previous efforts to utilize sapphire fiber sensors that can theoretically operate above 1650 °C have been limited because of the difficulty in implementing a sensor in an unclad and highly multimode fiber. Even with rigorous packing, fiber sensors can easily break down when subjected to large strains (e.g. 1%) or a shear force, causing serious challenges for sensor installation and operation [21]. Consequently, the applications of the optical fiber sensors are limited in heavy duty or large strain measurements which makes it difficult to be used in power plants.

In recent years, people have been migrating ideas of optical fiber to coaxial cable as they share the same electromagnetic theory. In comparison with optical fibers, main merit of using coaxial cable is its ability to survive large strains (more than 2%) due to its large dimension. Likewise, coaxial cables are also insensitive to lateral force or bending. Most of the optical sensing concept can be easily implemented on coaxial cables. The FBG concept has been successfully implemented on coaxial cables in 2011 [22]. A coaxial cable Bragg grating (CCBG) was fabricated by drilling open holes at a periodic distance along the coaxial cable. The periodic impedance discontinuities produce resonant peaks in both transmission and reflection spectra at discrete frequencies. This spectrum shifts whenever the CCBG is subjected to any physical change or change in their material properties. To demonstrate the ability to use CCBG as a sensor, they also conducted strain measurements. The large dynamic range, robustness and high resolution of coaxial cable Bragg grating (CCBG) sensor provide a very promising solution for structural health monitoring (SHM) [23, 24]. However, due to the long wavelength of the radio frequency, the CCBGs usually have a long grating length (~1 m) in comparison with FBGs (~1 cm), as a result, the spatial resolution of CCBG is limited.

Very recently, we presented a concept of high quality factor (Q-factor) coaxial cable Fabry-Perot resonator (CCFPR) with high measurement resolution, which is a promising solution for the spatial resolution problem of CCBG [22]. CCFPR consists of two highly reflective mirrors separated by a distance of centimeters. EM waves travelling inside the cable gets reflected from these two reflectors, resulting in a resonating pattern. When subjected to strain or temperature the physical length or material properties change, leading to a shift in the reflection spectrum[25] –[27]. This shift can then be used to determine the change in temperature or strain.

Although, CCFPR had several advantages, coaxial cables capability of operating at higher temperatures is limited by the melting point of dielectric, i.e. about 150 °C. To address this challenge, we, for the first time, report in this paper a hollow coaxial cable Fabry-Perot resonator (HCC-FPR) for high temperature sensing. In our HCC design, we have used air to replace the traditional insulator, as air is also a good dielectric insulator. A metal post, shorting the inner and outer conductor served as one of the reflector. A metal disk welded onto the end of the HCC served as the second reflector, thereby creating a resonating Fabry-Perot cavity leading to a resonating pattern. When the HCC-FPR is subjected to any physical change, e.g., thermal expansion, the reflection spectra shifts from its initial position, thus making HCC act as a sensor. The sensor structure, sensing principle, and calibration results are presented in the following sections.

2. THEORY

A schematic drawing of an HCC-FPR is shown in Fig. 1(a). A cross-sectional view of the HCC-FPR is also shown in Fig. 1(b). The HCC is homemade, which consists of an inner conductor, an outer conductor, and air in between serving as the dielectric layer. An HCC-FPR consists of two reflectors with very high reflectivity (> 80 %) separated by a distance of centimeters. A cylindrical metal post and a metal disk are used as the highly reflective mirrors by shorting the inner and outer conductor as shown in Fig. 1(a). The EM wave traveling inside the cable gets mostly reflected at the first reflector while a small portion (e.g. 1%) of the remaining energy with a phase shift gets transmitted and reaches the second reflector. At the second reflector, again most energy of the signal gets reflected and this repeats. The device physics was discussed in detail in our previous work [21]. Even though we have two reflectors with very high reflectivity here, still the transmission at particular resonant wavelengths/frequencies is 100%. These wavelengths/frequencies are those when the phase shift is equal to $2n\pi$. Then these partial waves travel back and forth in the cavity. The phase delay between two partial waves, which is attributed to one additional double trip is given by

$$\delta = \frac{4\pi d \cdot \cos\theta}{\lambda} = \frac{4\pi f d\sqrt{\varepsilon_r} \cdot \cos\theta}{c} \tag{1}$$

where λ is the wavelength; f is the frequency of the EM wave traveling inside the cable; θ is the angle between the transmitted and the incident wave; ε_r is the relative permittivity of the inner dielectric material of the cable and c is the speed of light in vacuum. As a coaxial cable is a transmission line supporting fundemental TEM waves, θ can be considered as zero.

The resonant reflection frequencies can be written as

$$f_m = m\frac{v_p}{2d} \tag{2}$$

where m is an integer and d is the length of the resonant cavity.

The spacing between two successive minima of the spectrum is defined as the free spectral range (FSR), can be expressed as

$$FSR = \frac{v_p}{2d} \tag{3}$$

When the spectrum shifts due to change in temperature, the resonant frequency shift can be given by

$$\Delta f_m = -(\sigma + \alpha_{CTE}) \cdot f_m \cdot \Delta T \ (Hz / ^\circ C) \tag{4}$$

where Δf_m is the change in frequency, ΔT is the change in temperature, σ is the temperature induced relative permittivity change of the air dielectric, α_{CTE} is the coefficient of thermal expansion of the stainless steel and f_m is the mth resonant frequency. The temperature measurement sensitivity for the developed sensor is $-(m \cdot v_p \cdot (\sigma + \alpha_{CTE})) / 2 \cdot d$, which is proportional to the harmonic number *m* and inversely proportional to the physical cavity length *d*. Thus, the shift in temperature can be determined by monitoring the change in resonant frequency.

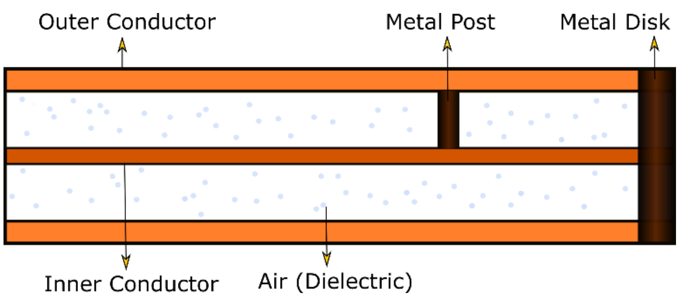

(a) Schematic Drawing of HCC-FPR

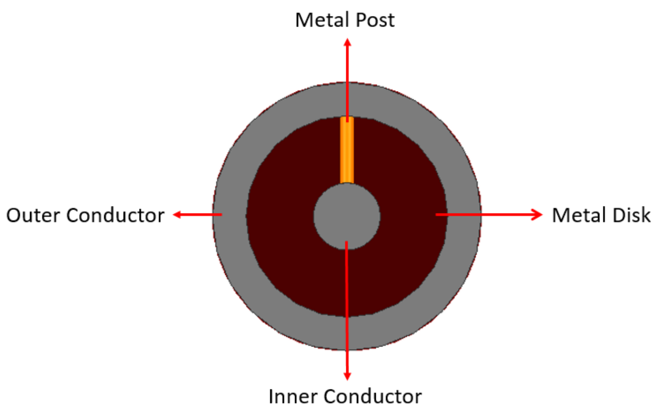

(b) Cross-sectional view of HCC-FPR.

Figure 1. Illustration of HCC-FPR.

3. EXPERIMENTAL SECTION

3.1 Fabrication of Sensor

The experimental setup of HCC-FPR for high-temperature sensing is schematically illustrated in Fig. 2. HCC is a homemade stainless steel coaxial cable, with air in between acting as the dielectric. The total length of the HCC is 1 meter. The diameter of the inner conductor is 6 mm. The outer and inner surface diameters of the outer conductor is 14 mm and 20 mm respectively. An FPR was engineered on the homemade HCC, by placing a metal post 100 mm away from the end of HCC and welding a metal disk onto the end of HCC, which was then designed to be connected to a commercial coaxial cable via an SMA to N-type connector. The diameter of the metal post and the thickness of the circular disk was 2 mm. The distance between the two reflectors was 100 mm. A vector network analyzer (VNA HP8753ES) was used to monitor the reflection spectrum during the temperature measurements. The VNA was configured for an observation bandwidth from 10 kHz to 4 GHz, a total of 1601 sampling points, and an intermediate frequency bandwidth (IFBW) of 300 Hz. All the machines used in this experiment was controlled using a laptop.

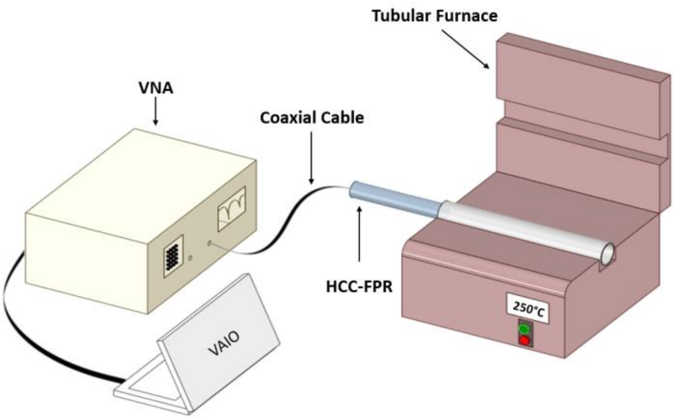

Figure 2. Experimental Setup of HCC-FPR.

Fig. 3 plots the measured reflection spectrum of a HCC-FPR. The fundamental frequency is observed at 1.42 GHz, followed by the first harmonic at 2.84 GHz. This experimental data matches the theoretical calculations of the fundamental and the expected harmonics from Eq. 2. The strength of the two resonant frequencies are approximately 7 dB and 4.5 dB. The first resonant dip has a higher strength (-7 dB) than second (-4.5 dB). One possible reason is that as frequency increases, the reflectivity of the first mirror decreases rapidly, whereas the reflectivity of the second mirror decreases gradually. The Quality-factors (Q-factors) are indicated in the plot for each resonant dip. Several ripples can be observed in Fig. 3. This is due to the multiple reflections incurred from the connector, coaxial cable, and port of the VNA.

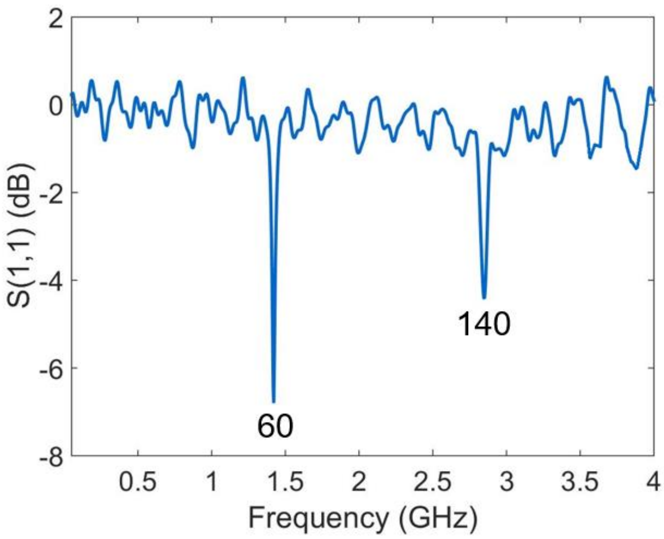

Figure 3. Experimental Results of Reflection Spectrum.

3.2 Temperature Measurement

To exhibit the capability of using HCC-FPR as a high-temperature sensing device, temperature measurement was conducted. The VNA was configured to acquire the resonant frequency of approximately 1.42 GHz with an observation bandwidth from 1.38 GHz to 1.44 GHz. The HCC-FPR was then placed in programmable tubular electric furnace for characterization of its capability for high temperature sensing (Fig. 2).

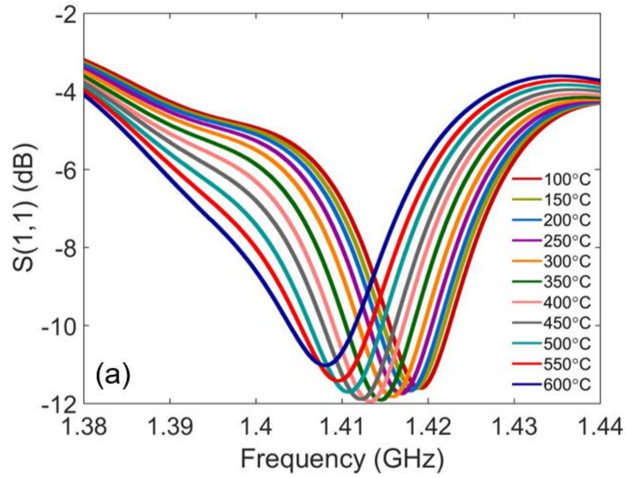

(a) Change in Reflection spectra as the ambient temperature increases

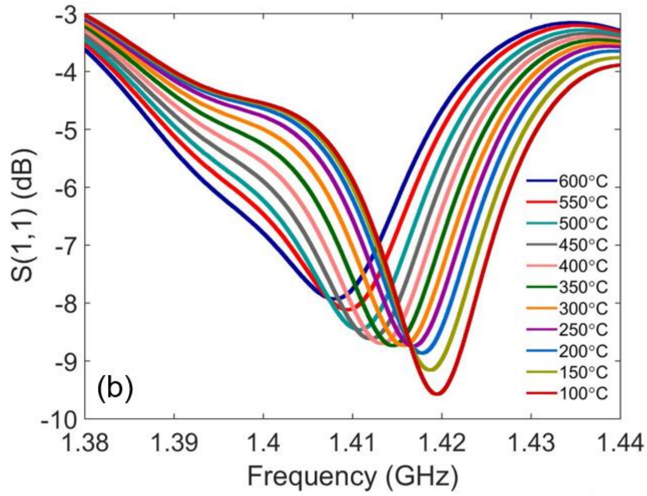

(b) Change in transmission spectra as the ambient temperature increases

Figure 4. Change in Reflection and Transmission spectra as the temperature increases.

Temperature was increased from 100°C to 600°C and then decreased back to 100°C at an incrementing/decrementing step of 50°C. For each temperature point, the reflection spectra was measured. Fig. 4 (a) and (b) indicates the shift in reflection spectra as the temperature increases and decreases. The spectra shift towards lower/higher frequency region as the temperature increases/decreases, indicating the effective electrical length of the cavity decreases/increases, correspondingly. The effective electrical length is related to the physical length between the two reflectors and the relative permittivity of the inner dielectric layer (air). The coefficient of thermal expansion for stainless steel is 10^{-5}/°C. The coefficient of thermal expansion for stainless steel is higher than the temperature induced relative permittivity change of the dielectric air, thereby dominating HCC-FPR response to temperature variations. At high temperatures, the Q factor decreases due to the increase of propagation loss between the two highly reflective reflectors and also due to low reflectivity at higher frequencies. Fig. 5 plots the change in resonant frequency as a function of temperature. Observed response was slightly non-linear.

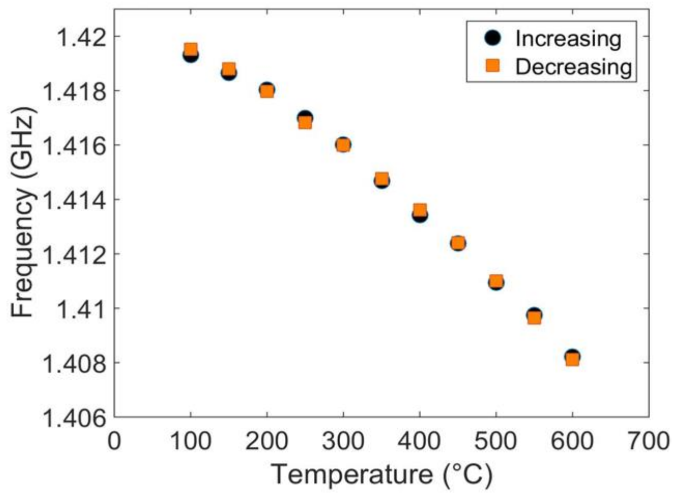

Figure 5. Resonant Frequency shift of the Reflection spectra as the temperature increases and then decreases.

The resonant frequency decreases as the temperature increases. The higher the temperature, the larger the temperature sensitivity becomes. The average temperature sensitivity of the HCC-FPR sensor was calculated to be -25 kHz/°C, demonstrating that this developed HCC-FPR can be used as a high temperature sensor with very good sensitivity. The temperature responses at the increasing and decreasing cycles also agreed well and showed no obvious hysteresis, indicating a good repeatability of the sensor. The stability of HCC-FPR was also characterized. The sensor was immersed inside a water filled beaker, and the resonant frequency was constantly recorded every 10 seconds for 40 minutes, which is shown in Fig. 6. The standard deviation was calculated to be approximately ±35 kHz, or a relative measurement resolution of 4.9×10^{-5} around 1.42 GHz. The results show great stability of the proposed sensor for temperature measurements.

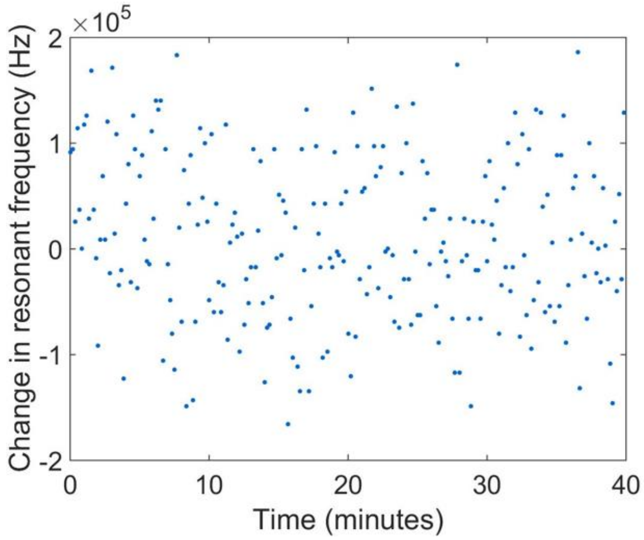

Figure 6. Measurement Resolution test at Resonant Frequency.

To further characterize the response of HCC-FPR sensor to temperature variation, the sensor was placed in the tubular furnace. The temperature was first increased in steps of 100°C from 100°C to 600°C and then decreased back to 100°C. Resonant frequency was recorded every 30 seconds for 30 minutes at each temperature point. Fig. 7 plots the recorded data. The proposed sensor demonstrated good stability at every temperature point and indicated good reversibility. The standard deviation at a constant temperature (e.g. 100°C) was calculated to be ±250 kHz, which is much higher than the standard deviation observed at ambient temperature in water (±35 kHz). A possible reason could be the drifting nature of the tubular furnace, tubular furnace can drift ±5°C at any given temperature. We can also notice that the response at each temperature step is a curve. One possible reason is the slow heating rate of the tubular furnace. Also, while decreasing temperature, it is difficult for the tubular furnace to keep the temperature constant at one point.

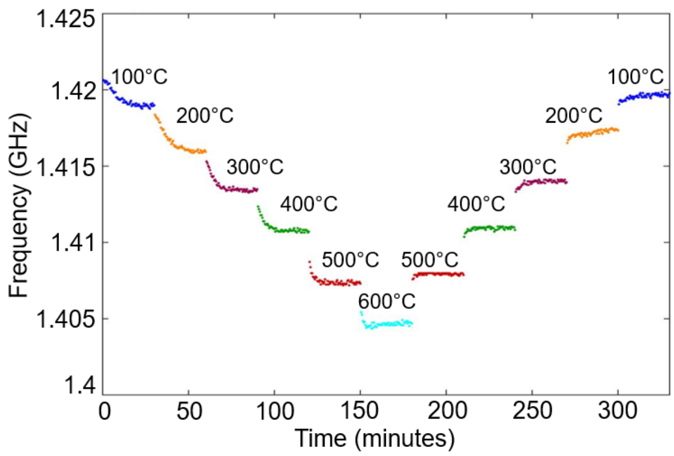

Figure 7. Resonant Frequency shift monitored at every temperature point.

4. CONCLUSION

This paper represents a low cost, robust HCC-FPR sensor for high temperature measurements. HCC was fabricated by replacing the traditional polyethylene dielectric insulator with air. A cylindrical metal post and a metal disk serves as two highly reflective mirrors. These reflectors result in an impedance discontinuity and the short circuit between inner and outer conductors results in very high reflections of the EM wave, thereby leading to a resonating pattern. When the cavity is subjected to temperature changes, the reflection pattern shifts. The sensor was tested from 100°C to 600°C showing great sensitivity, repeatability and stability for high temperature sensing. Though this paper was focused on using hollow HCC-FPR for high temperature sensing, it can also be used for strain and other types of sensing applications using different mechanical designs. HCC-FPR has many advantages like robustness, high spatial resolution, high finesse and large strain capability. These unique features can make HCC-FPR of great use in measurements of various parameters in high temperature harsh environments.

REFERENCES

[1] D. Lee *et al*, "Optical Fiber High-Temperature Sensor Based on Dielectric Films Extrinsic Fabry-Pérot Cavity," *IEEE Photonics Technology Letters,* vol. 26, *(21),* pp. 2107-2110, 2014.

[2] T. Stanczyk *et al*, "Electrolytic Joints Between Metal Surfaces and Metal-Coated Fibers for Application in High Temperature Optical Fiber Sensors," *Journal of Lightwave Technology,* vol. 33, *(12),* pp. 2480-2485, 2015.

[3] D. K. Qing and I.Yamaguchi, "Analysis of the sensitivity of optical waveguide chemical sensors for TM modes by the group-index method," *J. Opt. Soc. Am. B*, vol. 16, no. 9, pp. 1359-1369, 1999.

[4] J. Ctyroky, J. Homola and M. Skalsky, "Modelling of surface plasmon resonance waveguide sensor by complex mode expansion and propagation method," *Opt. and Quantum. Elec.*, vol. 29, no. 2, pp. 301-311, Feb 1997.

[5] R. Horvath, H. C. Pederson and N. B. Larsen, "Demonstration of reverse symmetry waveguide sensing in aqueous solutions," *App. Phys. Lett.*, vol. 81, no. 12, pp. 2166-2168, Sep 2002.

[6] J. Dostalek and J. Homola, "Surface plasmon resonance sensor based on array of diffraction gratings for highly parallelized observation of biomolecular interactions," *Sensor Actuators B*, vol. 129, no. 1, pp. 303-310, Jan 2008.

[7] X. Bévenot et al, "Surface plasmon resonance hydrogen sensor using an optical fibre," Measurement Science and Technology, vol. 13, pp. 118, 2002.

[8] Y. Dai, Y. Liu, J. Leng, G. Deng and A. Asundi, "A novel time-division multiplexing fiber Bragg grating sensor interrogator for structural health monitoring," *Opt. Lasers Eng.*, vol. 47, no. 10, pp.1028-1033, Oct 2009.

[9] J. Albert, L. Y. Shao and C. Caucheteur, "Tilted fiber Bragg grating sensors," *Lasers and Phot. Review*, vol. 7, no. 1, pp. 83-108, Feb 2012.

[10] N. Ni, C.C. Chan, W.C. Wong, L.Y. Shao, X.Y. Dong and P. Shum, "Cavity ring-down long period grating pressure sensor," *Sensors Actuators A*, vol. 158, no. 2, pp. 207-211, Mar 2010.

[11] M. Smietana et al, "Highly sensitive pressure sensor based on long-period gratings written in a boron co-doped optical fiber," Measurement Science and Technology, vol. 21, pp. 094026, July 2010.

[12] S. W. James and R. P. Tatam, "Optical fiber long-period grating sensors: characteristics and application," *Measurement Science and Technology,* vol. 14, *(5),* pp. R49-R61, 2003.

[13] J. Liu, Y. Sun and X. Fan, “Highly versatile fiber-based optical Fabry-Perot gas sensor,” *Opt. Express*, vol. 17, no. 4, pp. 2731-2738, Feb 2009.

[14] H. Sun, X. Zhang, L. Yuan, L. Zhou, X. Qiao and M. Hu, “An optical fiber Fabry-Perot interferometer sensor for simultaneous measurement of relative humidity and temperature,” *IEEE Sensors J.*, vol. 15, no. 5, pp. 2891-2897, May 2015.

[15] Y. Huang *et al*, "An extrinsic Fabry–Perot interferometer-based large strain sensor with high resolution," *Measurement Science and Technology,* vol. 21, pp. 105308, 2010.

[16] Y. Zhang *et al*, "Simultaneous measurement of temperature and pressure with cascaded extrinsic Fabry-Perot interferometer and intrinsic Fabry-Perot interferometer sensors," *Optical Engineering*, vol. 53, *(6),* pp. 067101-067101, 2014.

[17] Z. Tian *et al*, "Sourceless optical fiber high temperature sensor," *Optics Letters,* vol. 41, *(2),* pp. 195, 2016.

[18] M. Busch et al, "Inscription and characterization of Bragg gratings in single-crystal sapphire optical fibers for high-temperature sensor applications," Measurement Science and Technology, vol. 20, pp. 115301, 2009.

[19] J. Huang *et al*, "Microwave Interrogated Sapphire Fiber Michelson Interferometer for High Temperature Sensing," *IEEE Photonics Technology Letters,* vol. 27, *(13),* pp. 1398-1401, 2015.

[20] D. Lee *et al*, "Sapphire Fiber High-Temperature Tip Sensor with Multilayer Coating," *IEEE Photonics Technology Letters,* vol. 27, *(7),* pp. 741-743, 2015.

[21] J. Huang *et al*, "Interferogram Reconstruction of Cascaded Coaxial Cable Fabry-Perot Interferometers for Distributed Sensing Application," *IEEE Sensors Journal,* vol. 16, *(11),* pp. 4495-4500, 2016.

[22] T. Wei, S. Wu, J. Huang, H. Xiao, and J. Fan, “Coaxial cable Bragg grating,” *App. Phy. Lett.*, vol. 99, no. 11, pp. 113517(1-3), 2011.

[23] J. Huang, T. Wei, X. Lan, J. Fan and H. Xiao, “Coaxial cable Bragg grating sensors for large strain measurements with high accuracy,” *Sensors and Smart Structure Technologies for Civil, Mechanical and Aerospace Systems,* Apr 2012.

[24] J. Huang, T. Wei, S. Wu, X. Lan and J. Fan, “Coaxial cable Bragg grating sensors for structural health monitoring,” *Int. J. of Pavement Res. And Tech.*, vol. 5, no. 5, pp. 338-342, Sep 2012.

[25] M. F. Ahmed *et al*, "High Quality Factor Coaxial Cable Fabry-Perot Resonator for Sensing Applications," *IEEE Sensors Journal*, vol. 17, *(10)*, pp. 3052-3057, 2017.

[26] Y. Zhang *et al*, "Simultaneous measurement of temperature and pressure with cascaded extrinsic Fabry-Perot interferometer and intrinsic Fabry-Perot interferometer sensors," *Optical Engineering*, vol. 53, *(6)*, pp. 067101-067101, 2014.

[27] J. Huang *et al*, "A coaxial cable Fabry-Perot interferometer for sensing applications, *"Sensors (Basel, Switzerland),* vol. 13, *(11)*, pp. 15252-15260, 2013.

SECTION

2. CONCLUSION

To summarize, this thesis proposes two sensors: CCFPR, HCC-FPR for structural health monitoring applications. CCFPR is fabricated using low cost commercial coaxial cables, whereas HCC-FPR is fabricated using home-made hollow coaxial cable. In HCC, air replaces traditional dielectric polyethylene. Both CCFPR and HCC-FPR uses the same sensing concept i.e. FPR. Two highly reflective mirrors were introduced in the coaxial cables. EM waves travelling inside the cable gets reflected at the two mirrors resulting in a resonating pattern. When subjected to physical change or change in material properties, the resonating pattern shifts, thereby causing CCFPR, HCC-FPR to act as a sensor. The reflection coefficient of the different types of highly reflective mirror was calculated using finite element method. All theoretical results matched the experimental ones.

CCFPR was tested from 30 °C to 80 °C, showing great sensitivity and stability for temperature measurements. HCC-FPR was tested from 100 ° to 600 °C, showing great sensitivity, stability and reversibility for temperature measurements. Both CCFPR and HCC-FPR provided similar advantages like robustness, high spatial resolution, high finesse, high detection limit and large strain capability. CCFPR has very easy, low cost fabrication and installation. HCC-FPR can be used for ultra-high temperature harsh environments.

A high Q factor of 133 was recorded with a measurement resolution of 4×10^{-6} for CCFPR. CCFPR had several advantages like robustness, high spatial resolution, high finesse, high detection limit, large strain capability and can operate in temperatures as high as 150 °C. Also, CCFPR can be easily fabricated using the commercial coaxial cables, which results in easy installation and high cost reduction. HCC-FPR was fabricated using stainless steel HCC. However, we can also use high conductive metals like tungsten, nickel alloys, or conductive ceramics for fabrication HCC-FPR can operate in ultra-high temperatures as high as 1600 °C.

VITA

Mohammed Farhan Ahmed was born in Telangana, India in 1992. He received his Bachelor of Engineering (B.E.) degree in Electronics and Communication Engineering from Osmania University, Hyderabad, India, in 2014. He received his Master's degree in Electrical Engineering from Missouri University of Science and Technology in May 2018. He did an internship and co-op at Ansys Inc during the summer and fall semester of 2017. His research interests were mainly focused on the development of microwave devices and sensors for applications in Structural Health Monitoring.